



HAL
open science

Investigation of lipid modifications in J774 macrophages by vibrational spectroscopies after eicosapentaenoic acid membrane incorporation in unloaded and cholesterol-loaded cells

Sana Tfaili, Almar Al Assaad, Natalie Fournier, Fatima Allaoui, Jean-Louis Paul, Pierre Chaminade, Ali Tfayli

► To cite this version:

Sana Tfaili, Almar Al Assaad, Natalie Fournier, Fatima Allaoui, Jean-Louis Paul, et al.. Investigation of lipid modifications in J774 macrophages by vibrational spectroscopies after eicosapentaenoic acid membrane incorporation in unloaded and cholesterol-loaded cells. *Talanta*, 2019, 199, pp.54 - 64. 10.1016/j.talanta.2019.01.122 . hal-03484939

HAL Id: hal-03484939

<https://hal.science/hal-03484939>

Submitted on 20 Dec 2021

HAL is a multi-disciplinary open access archive for the deposit and dissemination of scientific research documents, whether they are published or not. The documents may come from teaching and research institutions in France or abroad, or from public or private research centers.

L'archive ouverte pluridisciplinaire **HAL**, est destinée au dépôt et à la diffusion de documents scientifiques de niveau recherche, publiés ou non, émanant des établissements d'enseignement et de recherche français ou étrangers, des laboratoires publics ou privés.



Distributed under a Creative Commons Attribution - NonCommercial 4.0 International License

Investigation of lipid modifications in J774 macrophages by vibrational spectroscopies after eicosapentaenoic acid membrane incorporation in unloaded and cholesterol-loaded cells.

Sana Tfaily ^a, Almar Al Assaad ^a, Natalie Fournier ^b, Fatima Allaoui ^b, Jean-Louis Paul ^b, Pierre Chaminade ^a and Ali Tfayli ^a

Abstract

Atherosclerosis is an inflammatory disease of the arterial wall caused by the formation of an atheroma plaque in the vessel wall. The uptake of modified LDL lipoproteins by sub-endothelial macrophages induces the latter's transformation into foam cells, which is the key step of atheroma plaque formation. The modifications of neutral lipids caused by foam cells formation are marked by the appearance of lipid droplets. Polyunsaturated fatty acids (PUFAs) incorporation into membrane phospholipids (PL) modifies their composition, which may influence membrane protein functions. The incorporation of eicosapentaenoic acid (EPA) reduces the anti-atherogenic ABCA1 (ATP Binding Cassette transporter A1) pathway and induces PLs modifications. In order to study lipids directly in the cell environment, a comparative study is conducted by vibrational spectroscopies on murine macrophages J774, loaded or not with cholesterol, which were enriched or not with eicosapentaenoic acid (EPA). The study enabled to identify changes in the spectral signature after cells enrichment with fatty acid (FA) relying only on chemometric analysis without deuterium labelling. Results highlighted spectral changes in the regions attributed to lipids associated to triglycerides, phospholipids and cholesterol in both Raman and IR.

Introduction

Atherosclerosis is the leading cause of morbidity and mortality worldwide and is responsible for most cardiovascular diseases (CVDs). It is a chronic and progressive disease characterized by the deposit of lipids and fibrous elements in the artery wall and can lead to an acute clinical event by obstruction of the arterial lumen and / or rupture of atherosclerotic plaque, calcification and thrombosis. The transformation of macrophages into foam cells (macrophages filled with lipid droplets) is responsible for the accumulation of lipids in the arterial wall [1]. Macrophages, derivatives of circulating monocytes, play a key role in atherogenesis by participating in the uptake of modified LDL (Low Density Lipoproteins) in the sub-endothelial cavity of the arteries through scavenger receptors. Unlike the classical LDL receptor, intracellular cholesterol content does not regulate scavenger receptor expression. This absence of regulation results in the formation of cholesterol-filled cells stored in the form of lipid droplets (LD) consisting mainly of cholesteryl esters (CE), which is the non-toxic storage form for the cells [2-4].

An elevated plasma LDL cholesterol level has been identified as one of the most important atherosclerosis risk factor. Oxidized low-density lipoprotein (Ox-LDL), generated by oxidative modification of trapped LDL in the vascular wall, is an important contributor to the atherosclerosis process [5].

Fournier *et al.* investigated the impact of the membrane incorporation of several polyunsaturated fatty acids (PUFAs) on ABCA1-mediated cholesterol efflux [6]. The latter is a key antiatherogenic pathway. Using different models of macrophages, authors reported that the incorporation of PUFAs in the phospholipids (PLs) membranes had different consequences depending on the type of macrophages, murine or human, and depending on whether the cells are overloaded or not in cholesterol. In the case of human macrophages in primary culture (HMDM: Human Monocytes-Derived Macrophages), the addition of eicosapentaenoic acid (EPA, C20:5 n-3) causes a significant modification of the composition of fatty acids (FA) of the PLs. This modification is due to the incorporation of EPA and its elongation product docosapentaenoic acid (DPA, C22:5 n-3) in the detriment of arachidonic acid (AA, C20:4 n-6) whose membrane concentration decreases. A significant decrease in ABCA1 (ATP Binding Cassette transporter A1) dependent cholesterol efflux accompanies this modification of composition without modification of the expression or location of the transporter. The deleterious action of the EPA on the functionality of the ABCA1 involves a reduction of the ATPase activity of the transporter via the protein Kinase A (PKA) pathway [6]. In addition, a study conducted in normal phase chromatography coupled to high-resolution mass spectrometry (LTQ-Orbitrap Velos Pro[®]) of

the phospholipidome of HMDM made it possible to build a model linking the variations of molecular species of PLs with the efflux of cholesterol and showed as a major impact an overexpression of phosphoinositol 18:0/22:5 in the decrease of efflux [7].

In cholesterol-loaded HMDM (foam cell model of atherosclerotic plaque), EPA addition revealed a decrease in ABCA1-dependent efflux without altering the expression or location of the transporter [8]. However, the detailed analysis of membrane lipid changes shows that the predictive model of efflux variations as a function of PLs molecular species is no longer valid in the foam cell model, suggesting that the mechanism responsible for alteration of efflux is different in this model. This observation is associated to the fact that the biological mechanisms are very different. EPA and the other tested PUFAs (AA, docosapentaenoic acid (DPA, C22:5 n-3) and docosahexaenoic acid (DHA, C22:6 w3)) reduce the efflux of free cholesterol by reducing the hydrolysis of the cholesteryl esters stored in the lipid droplets. This underlines the major importance of the cholesterol mobilization step for its efflux in the case of foamy macrophages. Fournier *et al.* have also reported that the lack of hydrolysis of cholesteryl esters involves neutral hydrolases of cytosol or neutral Cholesteryl Ester Hydrolase (nCEH) and not lysosomal acid hydrolase nor the autophagy of LDs. In addition, the importance of the reduction of CE hydrolysis and hence of efflux is positively correlated with the accumulation of cellular triglycerides (TG) also contained in lipid droplets, and not to the accumulation of CE. Moreover, the deleterious effect of EPA incorporation into PLs' membrane is not specific to the cholesterol release mediated by ABCA1 since the efflux of cholesterol mediated by CLA-1 (the human homologue of rodent Scavenger Receptor BI) or ABCG1 are also affected. Thus, it seems that the EPA (but also the other PUFAs, DHA, DPA and AA) leads to quantitative and / or qualitative modifications of LD lipids resulting in less hydrolysis of CE [8]. Majzner *et al.*, [9] studied the formation of lipid droplets by Raman spectroscopy in human endothelial cells in response to the uptake of PUFAs. Raman analysis in this study relied mainly on two vibrational bands at 1660 cm^{-1} (C=C stretching vibration in lipids and C=O stretching vibration in amide I; and at 3015 cm^{-1} (=C-H stretching mode in lipids) and the main interest was to evaluate how the modification in PUFA in the cell environment induces the LD formation. Results were confirmed by fluorescence microscopy [9]. Recently, Majzner *et al.*, evaluated the formation of lipid droplets upon to the uptake of various PUFAs in human endothelial cells by Raman imaging supported by atomic force microscopy (AFM). Among the tested PUFAs, a deuterated analog of arachidonic acid was evaluated. LD formation showed complex chemical composition depending on the used PUFAs [10]. Vibrational approaches based on label-free Raman analysis and Fourier transform infrared spectroscopy (FT-IR) allowed to characterize biochemical modifications in the case of non-alcoholic fatty liver disease [11]. The study was conducted on freshly isolated primary endothelial cells and hepatocytes from male mice fed with a high fat diet. Results showed alteration mainly in nuclei for endothelial cells and in cytoplasm for hepatocytes.

The present paper evaluates the investigation of lipid modifications by Raman and infrared vibrational spectroscopies in four different cell growth conditions. The murine macrophages (J774) are overloaded or not with cholesterol by acetylated LDL (acLDL) in presence or absence of EPA. Vibrational spectroscopies have the advantage to be non-destructive methods that can be applied to a small number of fixed or living cells. Our goal is to identify changes in the spectral signature following cells enrichment with fatty acid (FA). Spectra and spectral images are recorded *in vitro* after cell fixation. The expected changes are those of neutral lipids (CE and TG forming lipid droplets). According to the literature, different analytical tools of imaging have been used for the investigation of atherosclerosis. Some studies followed an *in vivo* approach, where measurements were directly performed on atherosclerotic plaques by ultrasound imaging [2], or by magnetic resonance imaging (MRI) [12] to follow the progression of atherosclerotic disease. Anatomical data provided by ultrasound present a low resolution and MRI data do not allow a characterization at the molecular level.

Other studies carried out *ex vivo* made it possible to record images on arterial segments. More specifically on autopsies performed 24 to 48 hours after death. The realization of these studies has made use of several analytical tools such as the fluorescence lifetime imaging microscopy [13]. The latter is non-invasive, allows the distinction of collagen levels and highlights the presence of lipids. However, fluorescence lifetime imaging microscopy does not permit to distinguish between different lipid classes. Studies on arterial segments were also conducted via vibrational spectroscopic methods in Raman [1] and in near infrared (NIR) [14]. Both techniques are suitable for *in vitro* and *ex vivo* studies. NIR allows the identification of chemical composition and provides molecular information. Chemical changes are detected in Raman, which is promising and opens a possibility for the diagnosis of atherosclerosis. However, the calcification attenuates

the signal in Raman and remains a limitative problem. Other researches focused on macrophages directly. These *in vitro* studies require cell culture of human monocytes / macrophages or mouse macrophages. Subsequently, images are acquired after cell fixation or directly on the cells in growth medium. For this, microscopy is mainly used, for example the scanning electron microscopy (SEM) [15]. SEM is conducted without sample labelling but does not allow quantifying the micro modifications at the level of the cell membrane, nor a molecular characterization. Spectroscopic techniques such as Raman vibrational spectroscopies [16] as well as Coherent anti-Stokes Raman spectroscopy (CARS) [17] were also exploited. In this context, researches introduced deuterium labels to distinguish the lipid molecules of interest among the large amount of lipids [16, 17].

It is trivial that the listed analytical techniques are more or less adapted according to the analyzed samples (atheroma plaques, arterial segment, cells). The sample preparation varies also upon to the method of analysis as well as the obtained information. Some techniques allow a macroscopic approach and permit to measure atheroma volume and progression. Other methods occur on a microscopic scale and are used to characterize biomarkers and permit to identify subtle chemical modifications.

As previously mentioned, our study aims to evaluate the potential of Raman and infrared techniques to investigate the lipid modifications on J774 macrophages in four different cell growth conditions relying only on chemometrics without deuterium labelling. This work was carried out using J774 mouse macrophages whose culture is easy and which offer the advantage of providing a large amount of cellular material in a very short time. The culture media conditions join the study of EPA membrane incorporation in unloaded and cholesterol-loaded macrophages conducted by Fournier *et al.*, [6, 8].

Materials and methods

Cell culture of J774 murine macrophages and general experimental design

Murine J774 macrophages are cultured in complete growth medium in 75 cm² flasks. Cells are maintained in a humidified atmosphere with 5% (v/v) of CO₂ at 37°C. The complete culture medium corresponds to RPMI-1640 containing antibiotics, 2 mM L-glutamine and 25 mM HEPES supplemented with 10% of heat-inactivated fetal bovine serum (FBS) (Thermo Fisher Scientific, Germany) [18].

Cells were seeded in 6-well plates (9.6 cm²/well) and four different growth conditions were studied. Into each well, we placed a CaF₂ window. We will distinguish between standard conditions where murine macrophages are supplemented or not with EPA, and two overloaded conditions where J774 supplemented with or without EPA were cholesterol-loaded by incubation with acetylated LDL. LDL isolated from plasma of individual normolipidemic donors was chemically modified by acetylation with the use of sodium acetate and acetic anhydride [19]. The well size and the duration of the culture cycle defined the concentrations of cells/mL.

To record Raman and infrared spectra on the same sample, J774 cells were fixed on thin CaF₂ windows with a thickness of 1 mm. Macrophages are known for their adherence property and no difficulty was encountered for cell attachment on CaF₂ surface.

Sample preparation for Raman and IR infrared analyses

1) Cells in standard media

For cell culture in standard media, 10×10⁴ cells/mL/well were seeded on CaF₂ window following the same steps as indicated above. The macrophages were then maintained and incubated at 37°C with 5% of CO₂ in 2 mL of complete culture medium per well. After 72h, the complete culture medium is replaced by the standard medium (STD) in three wells (3 slides) and by the medium supplemented with eicosapentaenoic acid EPA (Cayman Chemical Company, USA) at 70 μM in the three remaining wells (3 slides). After 30 h of incubation, the media were replaced by 2 mL of BSA-serum free medium (serum free medium supplemented with 0.2% BSA).

2) Cells in overloaded media

For cell culture in overloaded media, 7.5×10⁴ cells/mL/well were seeded on CaF₂ window. After 72h, the complete culture medium is replaced in 3 wells by the standard medium (STD) and by the medium supplemented with 70 μM of EPA in the other 3 wells. After 30h of incubation, media are replaced with STD and EPA media incubated with acetylated LDL at 75 μg/mL. Thirty hours later, these media are replaced by BSA-serum free medium.

Fixing cells on CaF₂ window

CaF₂ slides were delicately picked up from the wells. Cells were incubated with 2 to 3 mL of 4% paraformaldehyde (PFA) for 15 minutes. The PFA was then aspirated and the CaF₂ windows were washed with PBS (phosphate buffered saline) and then with distilled water. A first washing with 1.5 to 2 mL PBS eliminated the culture medium. Three washes with distilled water by filling 2/3 of the wells followed to prevent the deposition of PBS crystals.

Raman vibrational spectroscopy analysis

Acquisition of single spectra

Raman data are recorded via the Labspec 6 software on a Labram HR microspectrometer (Horiba Scientific, France SAS Villeneuve d'Ascq). The microspectrometer is equipped with an excitation He:Ne laser source operating at 632.81 nm excitation source (Toptica Photonics, Munich, Germany), a CCD detector (1024x256 pixels),) and a long focal microscope objective X100 LF with a numerical aperture NA of 0.9 (Olympus, Tokyo, Japan). The confocal pinhole was set at 200 μm and the slit aperture at 300 μm . Spatial (XY) resolution was around 1 μm^2 . A grating 300 grooves/mm permitted to collect data with a spectral resolution of 4 cm^{-1} . The acquisition time was set to 5 seconds with 10 accumulations over the interval 400-3800 cm^{-1} . The duration to record one spectrum is about 2 minutes. For each culture condition, three slides are analyzed. Seven cells are analyzed per slide and six spectra are recorded per cell. Among, three spectra are in the nucleus and three in the cytoplasm. In total, 126 spectra are recorded by culture condition. To these spectra is added the acquisition of the spectra of the culture media alone.

Raman imaging

Thanks to a motorized stage, cell Raman imaging was performed on the same device with a step of 1 μm . Acquisition parameters are the same as those defined to record single spectra apart from two parameters: the acquisition time and the autofocus. Autofocus is activated at the 980 to 1010 cm^{-1} spectral zone on each X, Y point (pixel of the image) to ensure a good focus of the laser on the surface of the sample. The acquisition time is a key parameter, its determination results from a compromise between the quality of the signal and the total recording time of the Raman images. For cells spectral imaging, the acquisition time was 5 seconds with 4 accumulations per spectrum. The time required to save an image depends on the size of the cell. The average duration was about 7 hours. Three images were recorded by growth condition. In total, 12 images of cells were acquired.

Infrared spectroscopy analysis

IR spectral images are recorded on a Spotlight 400 infrared spectrometer (Perkin Elmer Life Sciences, France) from 900 to 4000 cm^{-1} , with a pixel size of 6.25 x 6.25 μm^2 , and 16 scans per pixel. The spectral resolution is 4 cm^{-1} . Recording one image required, on average, 3 hours. The instrument is equipped with a 16-pixel detector cooled by liquid nitrogen. Before each acquisition, a background is recorded on a clean part of CaF₂ window (no cells) with a number of accumulations equal to 120. During the acquisition, the background is automatically subtracted from the spectra. Three mid infrared images are collected by growth condition. In total, 12 images of cells were acquired.

Data processing

Raman data processing

Smoothing and polynomial correction of the baseline are the first steps of preprocessing and were carried out using Labspec 6 (version 6.1.197, Jobin Yvon Technology, France). For single spectra, smoothing consisted on a three-degree polynomial Savitzky-Golay algorithm with a window of 12 points. For Raman imaging, "denoise" was chosen for smoothing with a factor of 3 and a window of 5 points. Baseline was corrected using a polynomial function of third order with a window of 12 points for the single spectra and 27 points for the spectral images.

Average spectra of cytoplasm and nucleus were calculated per slide, as well as average spectra of each growth environment. From the average spectra of J774 in standard and overloaded media and based on the literature, we proceeded to assign Raman characteristic bands.

Then, a simple subtraction of the different average J774 spectra two by two was carried out between the four growth conditions. This subtraction makes it possible to identify, if necessary, spectral regions allowing the discrimination between murine macrophages in different growth conditions.

Principal Component Analysis (PCA), preceded by standard normal variate correction, was performed using the SAISIR package in Matlab R2013b (The MathWorks Inc., USA).

For spectral images, the following steps describe the processing:

After smoothing and baseline correction, aberrant or low intensity spectra are removed. The projection of characteristic bands via Labspec 6 was performed. To reflect the relative distribution of lipids, the contribution of the 2800-2870 / 1645-1655 cm^{-1} band ratio was followed. The band at 2800-2870 cm^{-1} is attributed to ν_{sym} (CH_2) lipids [20], and 1645-1655 cm^{-1} zone corresponds to Amide I [21].

In addition, CLS fitting (Classical Least Squares) was carried out based on standard spectra (reference spectra). CLS calculates the abundance of known spectral signatures by linear regression. Average spectra in the nucleus and in the cytoplasm for each growth environment were defined as reference spectra. Besides, standard spectra, previously available from the laboratory database, were also used as for example the reference spectra of DNA, RNA and phospholipids.

Finally, a deconvolution conducted in the 1200-1400 cm^{-1} and the 2750-3160 cm^{-1} spectral zones enabled to observe the contribution of deconvoluted bands over the entire spectral image. An average spectrum per spectral image, and a second order derivative (degree 4, 17 points) carried out on all the average spectra, more precisely on two spectral regions (1200-1400 cm^{-1} and 2750-3160 cm^{-1}) were also calculated.

Infrared data processing

Mid-infrared spectra undergo first an atmospheric correction using Spectrum Image software (Perkin Elmer Inc., USA). An average spectrum for each culture condition is calculated. From these average spectra and based on the literature, we proceeded to the attribution of the infrared characteristic bands. Finally, an MSC correction (Multiplicative Scatter Correction) is performed in Matlab before computing PCA analysis.

Results

Bands assignment

Tables 1 and 2 present the vibrational bands and their assignments for Raman and infrared spectra respectively. Figure 1 illustrates the average of Raman spectral signature in J774 cytoplasm and nucleus for each growth supplementation condition and figure 2 displays the averaged IR spectral signature.

Raman bands assignment

Raman spectra in figure 1 appear to be identical at first sight. Nevertheless, a simple band attribution permitted to identify differences in the cytoplasm and nucleus spectral signatures between the different growth medium supplementations. Common bands corresponding to DNA appeared at 403-424 cm^{-1} , 661-680 cm^{-1} and 776-794 cm^{-1} spectral regions [21]. A band at 879-897 cm^{-1} corresponding to tyrosine and to desoxyribose nucleic acid ring is also observed. Vibrational bands from 1082 to 1103 cm^{-1} are also common to J774 in the different cell growth conditions. These bands represent the CC stretching (ν CC) of lipids and polysaccharides [21] and the ν (O-P-O) of DNA and RNA [22].

Two bands at 986-1014 cm^{-1} (ring breathing) and at 1019-1040 cm^{-1} ν (C-H) illustrate the phenylalanine, as well as bands at 1162-1185 and 1603-1618 cm^{-1} [20, 21]. Tyrosine vibrational bands appear at 640-644 cm^{-1} (C-C twisting), and through the doublet at 823-828 and 849-852 cm^{-1} , doublet is due to Fermi resonance between the ring-breathing vibration (symmetric stretching vibration). Bands at 880-894 cm^{-1} , 1171-1175 cm^{-1} correspond also to tyrosine [20, 21]. The symmetric breathing at 751 cm^{-1} corresponds to tryptophan and Raman bands at 1576, 1300-1309 and 1333-1337 cm^{-1} to adenine [21].

A highly intense band at 1655-1658 cm^{-1} represents Amide I and corresponds mainly to the carbonyl stretching (ν C=O) in peptide bonds [21] and to C=C stretching in lipids [23]. Amide I was observed for all spectra. Bands at 715-731 cm^{-1} δ (C-H) [21, 24] and at 1115-1130 cm^{-1} (ν C-C) [20] correspond to phospholipids. Bands associated to fatty acids appeared in the same spectral region, with weak intensity, such as bands at 715-731 cm^{-1} (C-H rocking), at 661-680 cm^{-1} (C=O-C deformation) and at 1019-1040 (C-H bending) [21, 24]. An intense band at 1425-1476 cm^{-1} corresponds to δ (CH) in lipids and proteins and is also attributed to cholesterol. Other bands are also assigned to cholesterol as vibrations at 686-708 cm^{-1} , 403-424 cm^{-1} and 532-548 cm^{-1} [20, 21].

Concerning differences in the fingerprint region from 400 to 1800 cm^{-1} , a shift in the maximum of the 394-440 cm^{-1} band is noted. The shape of this band, usually associated to DNA differs between standard (maximum at 408 cm^{-1}) and overloaded media (maximum at 420 cm^{-1}). The modification is explained by the presence of cholesterol in overloaded media, the vibrational band at 420 cm^{-1} corresponds to cholesterol. [20] In addition, the ring deformation at 700 cm^{-1} of cholesterol and cholesteryl ester [20, 24] is only detected on the J774 spectra of nucleus and cytoplasm in overloaded media.

The amide III band at 1223-1275 cm^{-1} , consisting on a combination of in plane deformation δ of N-H and C-H groups [25] and corresponding to the β -sheet conformation, highlighted dissimilarities. The width of Amide III band is broader in standard media (STD and EPA) compared to overloaded media (LDL and EPA/LDL). Difference in width suggests a shift, but is explained by the pronounced presence of the 1196-1223 cm^{-1} band corresponding to "random coil" conformation of Amide III [21].

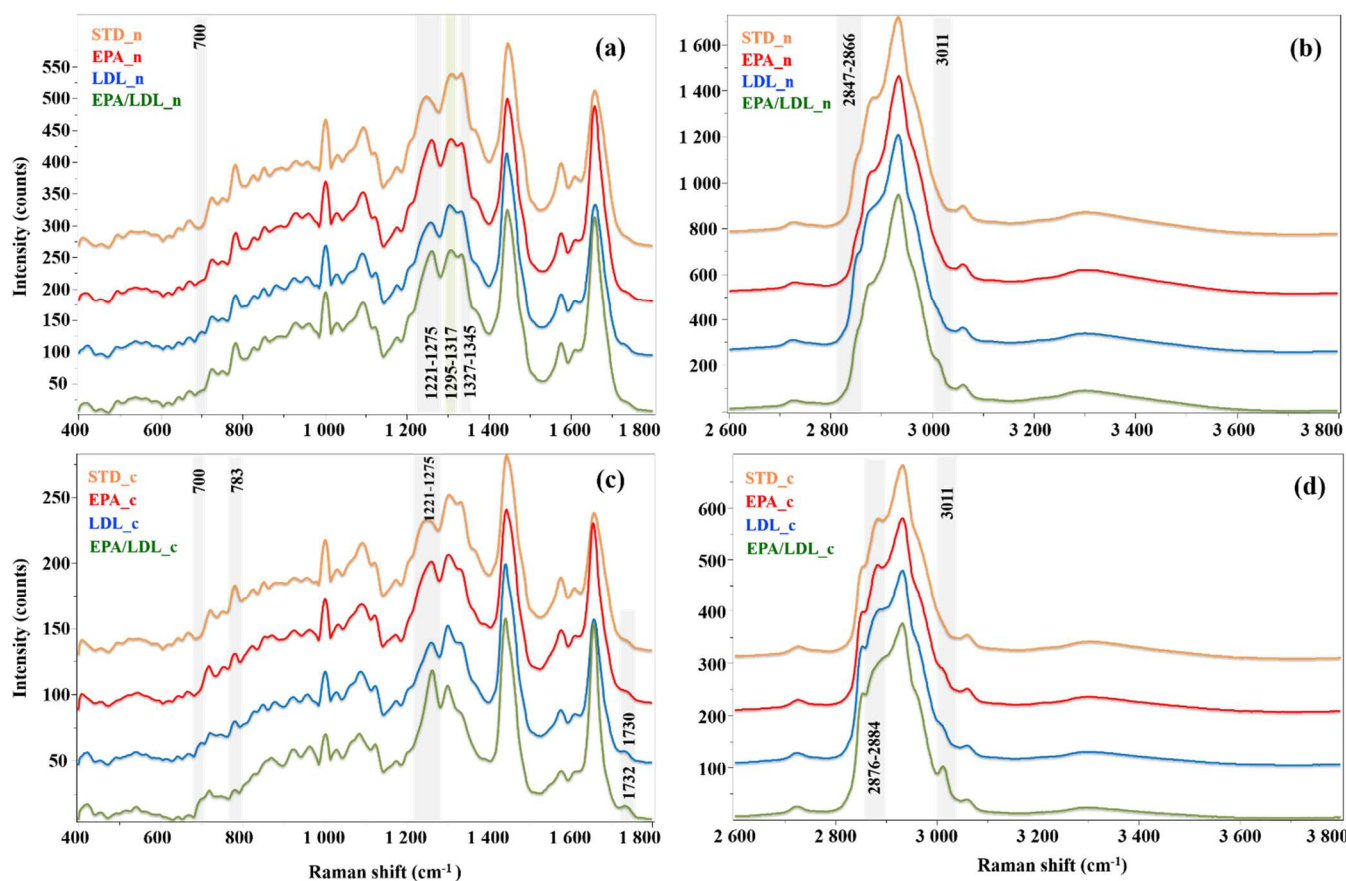


Figure 1: Raman average spectra of J774 murine macrophages in four growth conditions (standard conditions (STD and EPA) and overloaded conditions (LDL and EPA/LDL), in the nucleus (1a and 1b) and the cytoplasm (1c and 1d). The figure illustrates two spectral zones: the fingerprint region from 400 to 1800 cm^{-1} (a and c) and the lipid, protein and water region ranging from 2600 to 3800 cm^{-1} (b and d).

Moreover, the intensity of the ratio of 1295-1317 cm^{-1} to 1327-1345 cm^{-1} , corresponding to δ CH₂ of lipids and to ν CC and δ CH of polysaccharides respectively [21], indicated to be more important in the J774 cytoplasm compared to the nucleus regardless the culture medium environment. Another vibrational band at 1730 cm^{-1} assigned to the ν (>C=O) of triglycerides TG [24] revealed to be more

expressed in the cytoplasm spectra of J774 in overloaded media. The vibrational band assigned to phospholipids [21] at 783 cm⁻¹ in cytoplasm spectra of standard media was more expressed in standard media compared to LDL and EPA/LDL growth conditions.

Other differences concerned the lipids, proteins and water in the spectral region going from 2700 to 3600 cm⁻¹. The intensity of the band at 2847-2866 cm⁻¹ attributed to the ν_{sym} (CH₂) of lipids [21] was as expected higher in the cytoplasm spectra. The 2876-2884 cm⁻¹ band assigned to ν_{sym} (CH₃) of lipids [21] presents a larger shoulder and bandwidth in the cytoplasm for J774 spectra of overloaded media. Finally, the 3011 cm⁻¹ band corresponding to the ν (= CH) of TG and phospholipids [24] is more pronounced on the spectra of overloaded media, particularly on the cytoplasm spectra for EPA/LDL medium.

Table 1: Raman bands assignment from averaged spectra of J774 murine macrophages in four growth conditions (standard conditions (STD and EPA) and overloaded conditions (LDL and EPA/LDL).

v elongation or stretching, δ deformation, β bending, ρ rocking, τ torsion or twisting; *w*: weak, *m*: medium, *s*: strong and *vs*: very strong.

STD_n	STD_c	EPA_n	EPA_c	LDL_n	LDL_c	EPA/LDL_n	EPA/LDL_c	Raman band Assignment	Intensity
410	408	408	408					arginine, DNA [26] cholesterol [20]	w
				423	420	415	420		
454	456	454	457	455	453	454	453	probably polysaccharides skeleton [21]	w
496	496	496		493	493	496	493	ν (S-S) in proteins[21]	w
							515	phospholipids [20]	w
528	527	528						ν (S-S) trans-gauche-gauche in proteins, fatty acids [21]	
			543	538	540	538	541	β (CH ₂) bending, cholesterol [24], glucose-saccharide bond [20]	w
558	558	562		565	563	563		polysaccharides [20]	w
					612			cholesterol [20]	w
				617		617			
620	620	620	619					τ (C-C) proteins [20], phenylalanine[23]	
644	642	644	644	644	642	644	644	τ (C-C) tyrosine, cysteine[20]	w
669	669	671	666	669	669	671	669	T, G (DNA, RNA) [20]; δ (C = O - C) in FA [24]	w
							693	ν C-S in cysteine cholesterol, cholesteryl ester saccharides, polysaccharides [21]	w
700				700					
725	722	725	717	725	722	725	720	ν (C-H) phospholipids, rocking ρ (C-H) in FA chains, cytosine, thymine [20, 24]	w
751	751	751	756	751	746	751	748	DNA, symmetric breathing of tryptophan (protein) [20]	w
783	783	782	780	783	783	783	780	DNA ring breathing, phospholipids [21]	w
826	826	828	823	828	828	828	829	tyrosine (ring breathing) [20]	w
852	852	852	854	852	850	854		tyrosine (ring breathing and Fermi doublet) , (CC) in polysaccharides [21]	w
			871				870	ν (C - O - C) in FA, triglycerides TG [24]	w
	881			881	881			ρ (CH ₂) proteins [20]	
895	895	895				892		tyrosine, desoxyribose nucleic acid ring [21]	w
930	928	930	928	925	923	930	926	ν (C-C) probably amino-acids[20]	w
956	956	956	963	956	958	961	965	DNA, cholesterol [21] ν (C-C) proteins [20]	w
1001	1001	1001	1001	1001	1001	1001	1003	symmetric ring breathing of phenylalanine [21]	m
1031	1031	1031	1033	1029	1029		1029	ν (C-H) Phe, tyrosine, desoxyribose nucleic acid ring [21] β (CH ₂) in FA [24]	w
				1059	1061		1059	ν (C-C) lipid skeleton [20]	w
1091	1091	1093	1091	1091	1089	1093	1084	ν (C-C) lipids, polysaccharides [21] ν (O-P-O) in DNA/RNA [22]	m
1125	1125	1124	1123	1123	1123	1125	1123	ν (C-C) lipids : trans hydrocarbon chain, polysaccharides [21, 24] ν (C-N) of proteins, ν (C-O) of carbohydrates [27], cytochrome C [28]	w
1174	1174	1176	1174	1176	1174	1176	1176	cytosine/guanine [20] , ν (C-H) Tyr, Phe [21]	w
1203	1205	1205		1202	1200	1207	1201	ν (C-C ₆ H ₅) tryptophan, phenylalanine [20]	w
1248	1248	1253						Amide III (random coil)	m

			1260	1257	1260	1260	1262	v P=O phospholipids (1249 cm ⁻¹) Amide III [21] , Combination of δ (N-H) and δ (C-H) in β -sheet [29]	
1309	1302	1311	1302	1305	1300	1307	1300	δ (CH ₂) lipids, adenine and cytosine in DNA/RNA [21]	m
1334	1331	1334	1335	1331	1336	1334	1335	v CC, δ CH Phe, Trp, polynucleotide chain (DNA purine bases), adenine, guanine, RNA, polysaccharides [21]	w
1369	1369	1369		1375		1371		ν_{sym} (-COO) [29]	w
1446	1444	1446	1444	1442	1442	1444	1442	δ (CH) proteins and lipids (fatty acids at 1438, cholesterol at 1440) [21]	s
1577	1577	1577	1577	1577	1577	1577	1577	guanine, adenine ring stretching [30]	w
1609	1609	1611	1611	1611	1611	1611	1611	δ (C=C) in plane, Phe and Tyr [20, 21]	w
1658	1658	1658	1656	1658	1658	1658	1658	v (C=O) amide I [20, 21] and v(C=C) lipids [23]	s
	1730	1730	1730	1732	1730	1730	1732	v (>C=O) ester bond in TG[24]	w
2727	2725	2729	2725	2725	2723	2727	2723	ν_{sym} (C-H) lipids[20]	w
2850	2855	2853	2852	2852	2853	2851	2853	ν_{sym} (CH ₂) lipids[21]	w
2879	2885	2877	2883	2875	2884	2876	2876	ν_{asym} CH ₂ proteins [21]	vs
2932	2932	2934	2932	2932	2932	2932	2932	ν_{sym} (CH ₃) lipids [21]	w
			3011			3011	3011	v(=CH) TG and phospholipids [24]	w
3059	3059	3059	3060	3059	3059	3061	3059	v(=CH) lipids [24]	w
3303	3303	3300	3303	3301	3298	3298	3298	v(N-H) proteins[29], v(O-H)	w

IR bands assignment

Infrared and Raman spectroscopies provide complementary information [21]. For all IR spectra and regardless the growth medium supplementation, vibrational bands of low intensity assigned to DNA appeared in the following intervals: ν (PO₃²⁻) at 965 cm⁻¹, ν (C-O) at 1055-1070 cm⁻¹ and ν_{sym} (PO₂) 1084 cm⁻¹. DNA presents also a band of medium intensity assigned to ν_{asym} (PO₂) [21, 31]. A highly intense amide II band, assigned to δ (N-H) deformation coupled with the ν (C-N) stretching, is also detected at 1545 cm⁻¹. At 1653 cm⁻¹, vibrational band assigned to the ν (C=O) coupled with the ν (C-N) and the δ (N-H) of the amide I is also identified [21]. A list of lipid bands is also identified. At 1450 cm⁻¹, appears the vibrational IR band assigned to the δ (CH₃) of lipids. The bands at 2850, 2920 and 2956 cm⁻¹ assigned respectively to the ν_{sym} (CH₂), ν_{asym} (CH₂) and ν_{asym} (CH₃) of lipids and fatty acid chains are also present [31, 32].

In the fingerprint region ranging from 900 to 1800 cm⁻¹, some differences appear according to the supplementation of growth medium: the vibrational band at 1732 cm⁻¹ attributed to the ν (C=O) of CE, FA and polysaccharides [21, 33] is more expressed for J774 in overloaded media. This band is also present on the spectrum of J774 enriched with EPA.

In the lipid region ranging from 2800 to 3600 cm⁻¹, the ratio between the ν (N-H) band at 3220 cm⁻¹ and the band at 3280-3300 cm⁻¹ corresponding to Amide A: Fermi resonance of ν (N-H) with amide II, and to bonded OH stretching ν (O-H) [21] is reversed between STD, EPA and EPA/LDL growth environments compared to the LDL loaded medium.

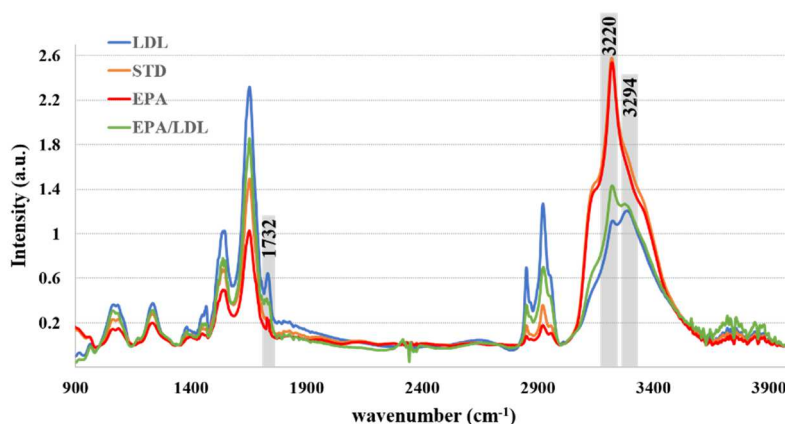


Figure 2: Mid-infrared spectra (average spectra) of J774 murine macrophages in four growth conditions (standard conditions (STD and EPA) and overloaded conditions (LDL and EPA/LDL)).

The band at 3280-3300 cm^{-1} is present for all J774 IR spectra despite the growth medium supplementation; the band's width is broader on the spectra of the LDL loaded medium with a shift of about 10 cm^{-1} of the maximum. This shift is also observed in EPA/LDL medium where the maximum is at 3284 cm^{-1} . However, the intensity of 3280-3300 cm^{-1} band for J774 in EPA/LDL supplemented medium is significantly lower, compared to the other three supplementation conditions. And the maximum of the band 3280-3300 cm^{-1} is at the level of 3294 cm^{-1} for standard media.

Table 2 Assignment of IR characteristic bands from average spectra of J774 murine macrophages in four growth conditions (standard conditions (STD and EPA) and overloaded conditions (LDL and EPA/LDL).

v stretching, δ deformation, γ wagging; w: weak, s: strong; vs: very strong.

STD	EPA	LDL	EPA/LDL	Assignment	Intensity
965	965	965	965	ν (PO_3^{2-}) DNA, RNA ribose[31], C-C desoxyribose in polysaccharides[21]	w
1063	1065	1060	1061	ν (C-O) DNA, RNA ribose[31]	w
1085	1084	1084	1084	ν_{sym} (PO_2^-) DNA, RNA, phospholipides[31], ν (C-O-C) β -glucose[21]	w
1172	1172	1172	1172	ν_{asym} (C-O) ester of phospholipides, CE[31, 32]	w
1234	1234	1234	1234	ν_{asym} (PO_2^-) DNA, RNA, phospholipides[21, 31]	m
		1385	1385	γ_{sym} (CH_3) phospholipides, FA, TG[31]	w
1394					
	1398			δ (CH_3), ν (C=O) lipids, proteins[31]	
1450	1450	1450	1450	δ (CH_3) lipids, proteins[31]	w
1545	1544	1545	1546	Amide II : δ (N-H) coupled to ν (C-N)[21]	s
1653	1651	1653	1653	Amide I : ν (C=O) coupled to ν (C-N) and δ (N-H)[21]	vs
	1732	1732	1732	ν (C=O): lipids, CE, FA ⁴⁶	w
				ν (C=O) in COOH of polysaccharides [21]	
2852	2850	2850	2852 (w)	ν_{sym} (CH_2) lipids, fatty acids chain [31, 33]	m
2922	2920	2922	2922 (w)	ν_{asym} (CH_2) lipids, fatty acids chain [31, 33]	s
2958	2956	2956	2954	ν_{asym} (CH_3) lipids, CE, FA [16]	w
3220	3220	3220 (w)	3218	ν (N-H) [21]	s
3294	3294	3284 (m)	3284	Amide A: Fermi resonance of ν (N-H) with amide II, bonded OH stretching ν (O-H) [21]	w

Investigation of J774 Raman spectral signature

Spectra subtraction

Averaged J774 spectra are subtracted two by two (Figure 3). The difference between spectra in overloaded (LDL or EPA/LDL) and standard media (STD or EPA) highlighted possible modifications in the spectral signature in function of the growth medium environment. The expression of vibrational bands at 2847-2866 cm^{-1} and 2884-2910 cm^{-1} [21] respectively assigned to symmetrical CH_2 stretching of lipid and asymmetric stretching of protein is more important in overloaded media, as well as the expression of the 700 cm^{-1} (686-708 cm^{-1}) band attributed to cholesterol and polysaccharides [21]. Other intervals including bands assigned to CH_2 twisting in lipids at 1280-1330 cm^{-1} and to CH_2 scissoring in lipids at 1426-1490 cm^{-1} [21] showed an overexpression in overloaded media. The spectrum resulting from the subtraction illustrates an interesting band at 1632-1706, probably corresponding to double bond stretching in lipids ν (C=C) [21, 24]. Supplementation of the growth medium with fatty acids (EPA, LDL or EPA/LDL) highlights a change in the 3011 cm^{-1} band. This band corresponds to the (=CH) stretching of TG and PLs [24] and is highlighted after the addition of FA in medium. Results of subtraction showed that the spectral changes are more important in the cytoplasm.

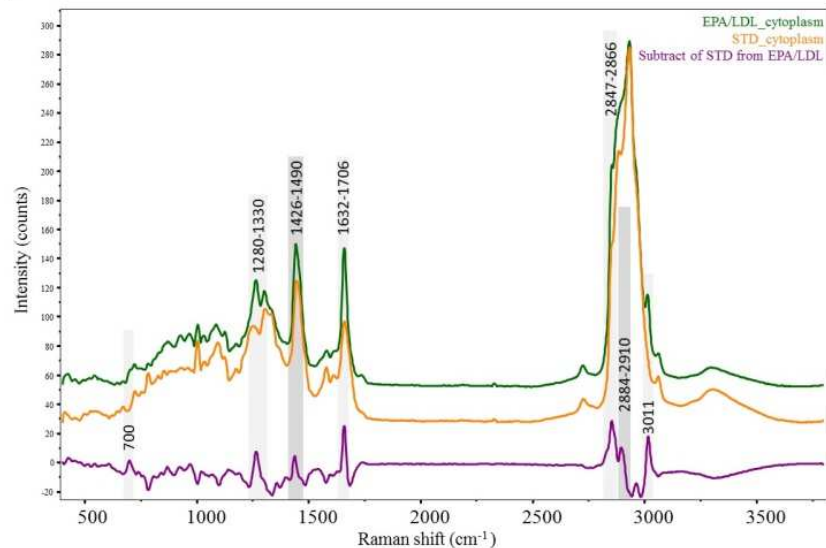


Figure 3: Example of spectral subtraction of J774 spectra in the cytoplasm, J774 spectrum in STD medium subtracted from spectrum in EPA/LDL medium.

Relative distribution of characteristic bands and CLS fitting

Figure 4 illustrates J774 spectral images and the contribution of the ratio $2700-2800 / 1645-1655$ ($v_{sym}(CH_2)$ of lipids / Amide I) [20, 21, 23]. Results point out a higher lipid ratio in the cytoplasm of cells in overloaded media (LDL and EPA/LDL). Enrichment of growth medium with EPA alone does not reveal a modification in the lipid ratio. J774 cell in EPA/LDL medium shows the highest lipid content among the four tested growth medium supplementations. Results of CLS fitting reveal a higher ratio in the nucleus also, a modification in the lipid content in the nucleus of J774 in EPA/LDL medium is observed.

For CLS fitting, reference spectra of PLs, DNA, RNA, EPA and LDL as well as two spectra representative of J774 cytoplasm and nucleus are used. Figure 5 displays murine macrophage spectral image in EPA/LDL medium and. EPA, LDL and phospholipids indicate a greater contribution in the cytoplasm. Although the distribution of EPA and LDL is mainly detected in cytoplasm. Their impact on the lipid content of the nucleus can be observed (Figure 5). Lipids presence is known in the nuclear envelope but the nucleus also contains lipids which are located further inside.[34]

Second order derivatives

Second order derivative allows a better display of band overlaps and highlights dissimilarities in spectral signature. For each spectral image and each growth medium, an average spectrum is calculated and second order derivative is then conducted on two spectral regions: $1200-1400\text{ cm}^{-1}$ and $2750-3160\text{ cm}^{-1}$.

In the $1200-1400\text{ cm}^{-1}$ interval (Figure 4), vibrational bands at 1245 and 1249 cm^{-1} assigned respectively to the random coil conformation of amide III and to $\nu(P=O)$ in phospholipids [21] are only present for spectra of overloaded media, and are more relevant for J774 in LDL medium. The band around $1297-1312\text{ cm}^{-1}$ attributed to $\delta(CH_2)$ in lipid [21] is only present in spectra of overloaded media. As a result, the width of the band at 1325 cm^{-1} corresponding to $\delta(C-H)$ of proteins [21] looks narrower for spectra of J774 in standard media but it is only the effect of side to side overlapping bands.

In the spectral interval ranging from 2750 to 3160 cm^{-1} (Figure 4), second order derivative spotted differences related to growth medium conditions. Vibrational band at 2823 cm^{-1} , $\nu(CH_2)$ of FA [24], is more marked on the spectra of overloaded media. Band at 2884 cm^{-1} assigned to νCH_2 of phospholipids [21] figures out only for LDL medium, while band at 2916 cm^{-1} assigned to $\nu(CH_3)$ in TG [35] is present on all spectra except spectra of LDL medium. The ratio $2950-2976 / 2978-2994\text{ cm}^{-1}$ is greater when media are overloaded with fatty acids. The 3011 cm^{-1} band corresponding to the $\nu(=CH)$ of FA and PLs [24] is present in standard EPA medium and overloaded LDL medium, probably following the enrichment of media with FA, but is more expressed for J774 in EPA/LDL overloaded medium.

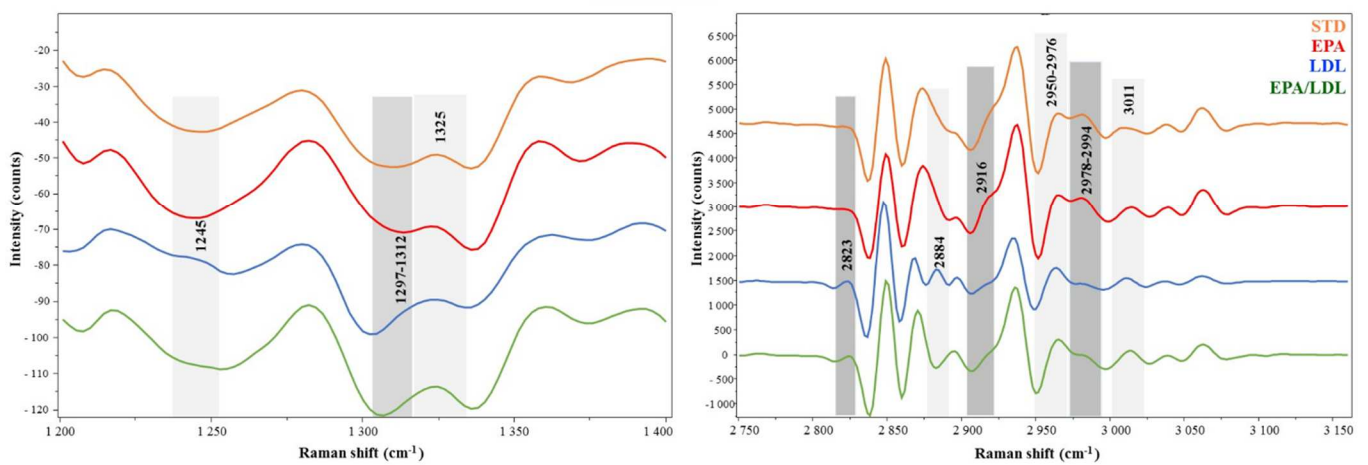
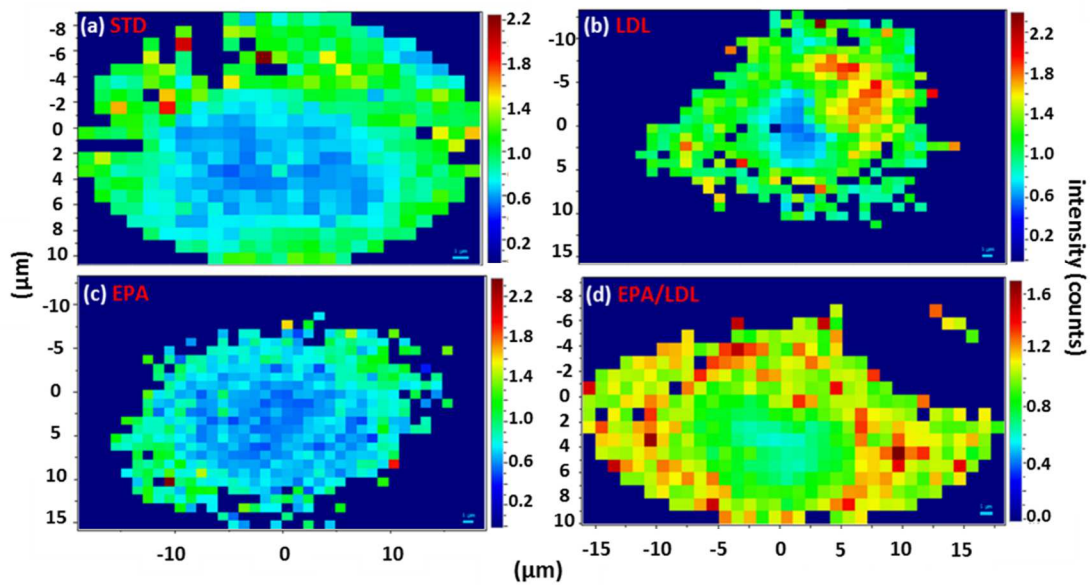


Figure 4: Projection of the ratio between the bands at $2800\text{--}2870\text{ cm}^{-1}$ (lipids) and $1645\text{--}1655\text{ cm}^{-1}$ (Amide I) on the Raman spectral images of J774 showed to be higher in the cytoplasm of J774 in overloaded growth media (4b and d). And second derivatives calculated on mean J774 spectra for different growth conditions considering two spectral zones: $1200\text{--}1400$ and $2750\text{--}3160\text{ cm}^{-1}$.

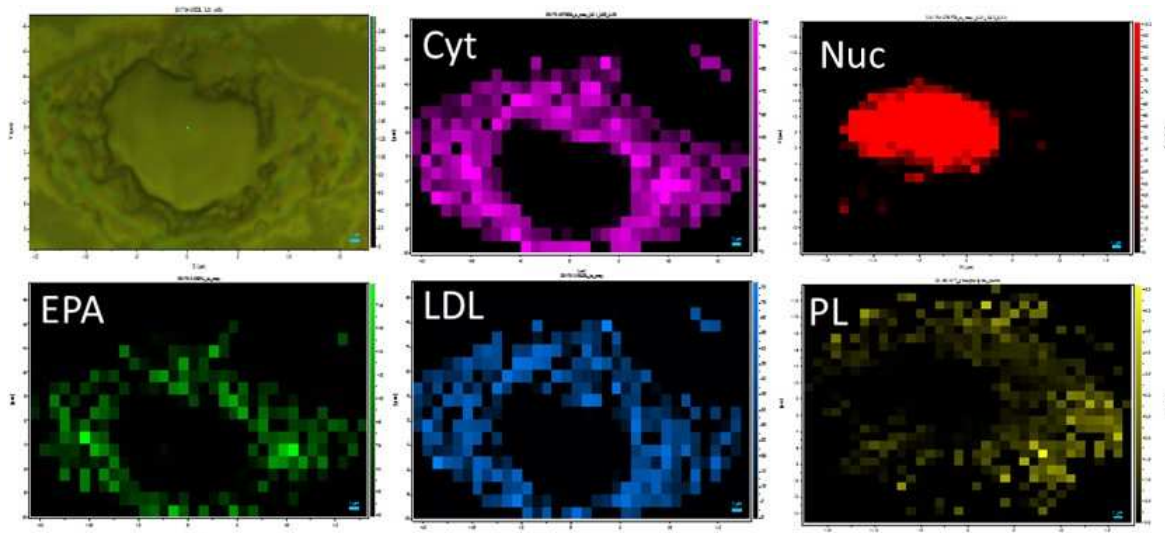


Figure 5: Visible image of J774 cell in EPA/LDL growth medium and Raman spectral images after CLS fitting using reference spectra of cytoplasm, nucleus, EPA, LDL and PL.

Principal component analysis

Principal component analysis is carried out on pretreated Raman spectra. Pretreatment consisted on baseline correction and spectra smoothing. Letter "A" designates the principal components and is followed by the component number. The first six components represent 96.6% of the information. First component represented around 76% of the information and second component around 12%. Score plot on the first two components (A1 and A2) permitted to distinguish spectral signature in the nucleus from signature in the cytoplasm, but did not reveal clusters illustrating different growth media (Figure S1 in supplementary data). In addition to score plots, centroids are illustrated for each group with 95% confidence ellipse drawn around. Groups are related to cell compartment (cytoplasm (c) and nucleus (n)), or defined with respect to growth conditions STD, EPA (standard media), LDL and EDL (overloaded media). EDL stands for EPA/LDL in PCA graphics.

Score plot on A1 (75.8%) and A3 (4.6%) allows the distinction between standard and overloaded media according to the third component (Figure S2 in supplementary data). The score plot on A2 and A3 brings almost the same information as on A1 and A3. This difference between standard and overloaded media is slightly improved on A1 and A4. Score plot on A2 and A4 brought the same information as the projection on A1 and A4. This confirmed that the components A1 and A2 provided information related to cell compartment and not to growth medium. Score plot on A3 and A4 components discriminates between standard and overloaded media. Score plot on A4 (3.2%) and A6 as well as the projection of the centroids (Figure S3 in supplementary data) give the same information. A6 contributes only to 0.2% of the information, but the loading of A6 is a marker for the presence of eicosapentaenoic acid in the medium. A6 clearly helps to distinguish the EDL medium from the other three, EPA correlates slightly with the positive part of A6 axis (Figure 6). Score plots with component A5 are not shown as the A5 loading reveals fluorescence and noise.

Loading plots confirmed observations pointed previously in data processing. The eigenvector of A1 has a negatively correlated band at 2824-2865 cm^{-1} (Figure 6). This band assigned the $\nu_{\text{sym}}(\text{CH}_2)$ of lipids [21] is more present in the cytoplasm than in the nucleus and this is confirmed from the score plot on A1 and A2 (Figure 6 and S1 supplementary data). The loading of A2 shows that the band at 1310-1365 cm^{-1} corresponding to the ν CC and the δ CH in polysaccharides [21] correlates positively (Figure 6). This band is more important on the spectra of the nucleus. The loading plots of A1 and A2 confirmed that both components give information related to the cell compartment.

Bands, which appeared to be more intense in overloaded media, are positively expressed on the eigenvector of A3 (data not shown) and A4. For example, bands at 691-728 cm^{-1} (Cholesterol, Cholesteryl ester and polysaccharides) [21], at 1413-1475 cm^{-1} ($\delta(\text{C-H})$ in proteins and lipids (including cholesterol at 1440) [21]), at 1620-1693 cm^{-1} (ν (C=O) in Amide I [20, 21] and $\nu(\text{C=C})$ in lipids [23]), and at 1717-1747 cm^{-1} ($>\text{C=O}$ stretching bond in TG) [24]. These vibrational bands have the same contribution on A4 (Figure 6).

In addition, three other bands correlate positively on A4. For example, the 398-435 cm^{-1} band assigned to DNA [26] and cholesterol [26]; the 2804-2908 cm^{-1} band which corresponds to the $\nu_{\text{sym}}(\text{CH}_2)$ in lipid [21] and the band at 2997-3020 cm^{-1} attributed to the $\nu(\text{=CH})$ of TG [24]. These characteristic bands, relevant in overloaded media, correlate with A4. Overloaded media are projected onto the positive part according to A4 axis in the score plot on A1 and A4 (Figure S2 in supplementary data).

A6 loading positively expresses the bands at 691-728 cm^{-1} , 1413-1475 cm^{-1} , 1620-1693 cm^{-1} and 1717-1747 cm^{-1} . Bands that are the most expressed on this loading are the 1244-1287 cm^{-1} band assigned to ν P=O in phospholipids and to Amide III and the band at 2997-3020 cm^{-1} (Figure 6).

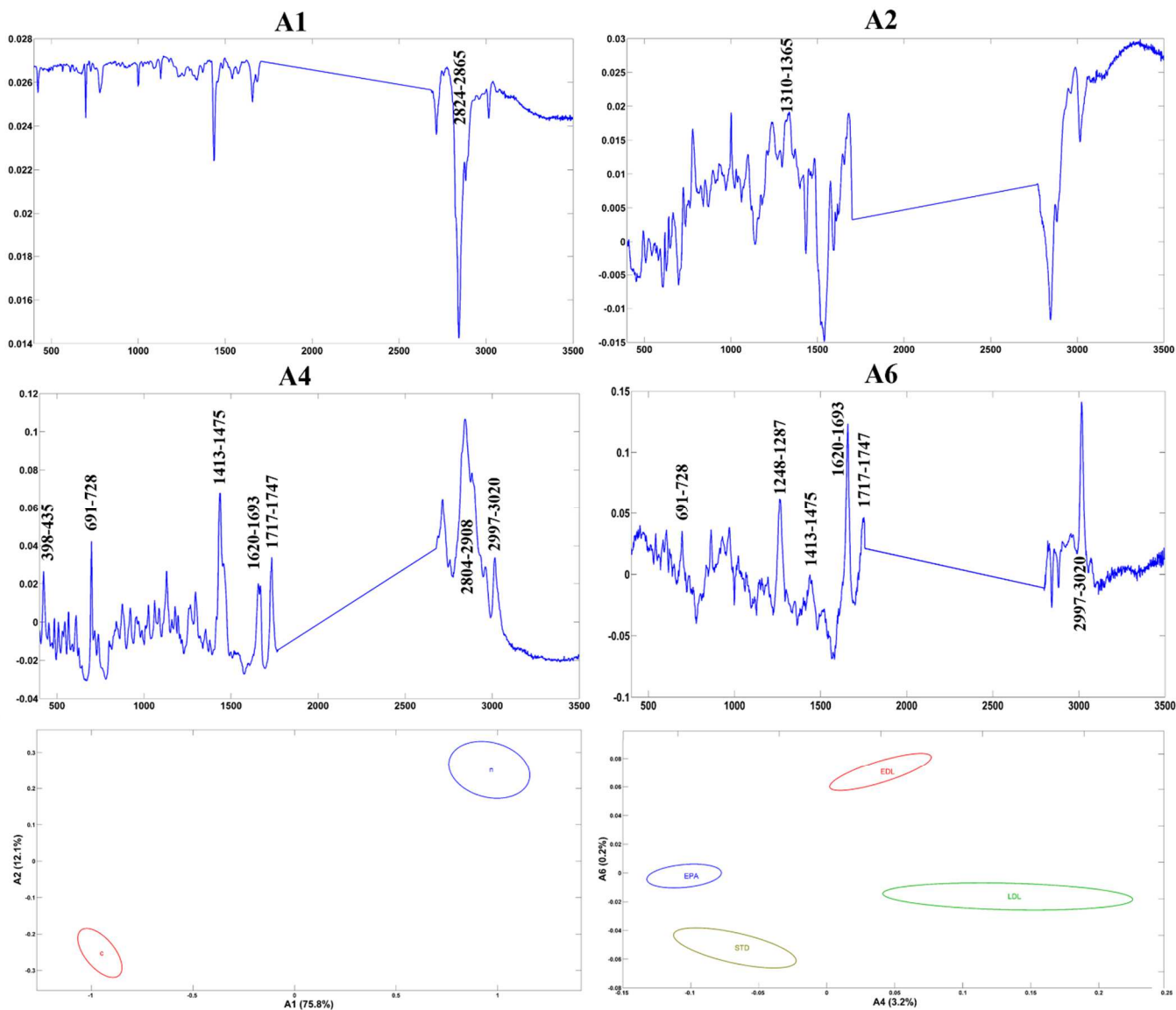


Figure 6: Loadings of principal components A1, A2, A4 and A6 for Raman data. Projection of the confidence ellipses of centroids for cytoplasm and nucleus in the space of principal components A1 and A2, and for the different growth conditions in the space of A4 and A6. On the plot, 'c' and 'n' respectively denote the cytoplasm and the nucleus, STD, EPA, LDL and EDL are the different culture conditions. EDL stands for EPA/LDL in PCA graphics.

Investigation of J774 IR spectral signature

For IR data processing, we performed PCA on pretreated spectra. Pretreatment consists on a Multiplicative Scatter Correction (MSC) MSC eliminates baseline shift and allows spectral scaling. It provides a better correction of the baseline and corrects the slope by using a reference spectrum. The reference spectrum is the average spectrum of the dataset.

According to the score plot and to the 95% confidence ellipses of centroids in the space of A1 (62.4%) and A2 (19.1%), the first component provides information related to the presence of the eicosapentaenoic acid EPA in the medium. The second component makes it possible to distinguish the spectra of the LDL medium from other growth media (Figure S4, b in supplementary data).

For loading plots, we cut the spectral region between 1800 and 2700 cm^{-1} as it contains no data. Thus, a straight line appears in this region for all loadings. A1 loading brings out the band at 1166-1199 cm^{-1} assigned to $\nu_{\text{asym}}(\text{C-O})$ of phospholipid esters, and cholesteryl ester [31, 32] (Figure 7, I). The latter is expressed positively on A1 eigenvector and is probably related to the presence of EPA in the medium (EPA or EPA / LDL). The 3278-3340 cm^{-1} band (Amide A: Fermi resonance of $\nu(\text{N-H})$ with amide II, and bonded $\nu(\text{O-H})$) [21] is negatively correlated

on A1 loading and reflects the observed changes in J774 spectra in LDL medium. LDL spectra are projected on the negative part of A1 axis in the score plot on A1 and A2 (Figure S4, a and b in supplementary data).

The eigenvector of A2 reveals a positive correlation of the band 3278-3340 cm^{-1} and confirms the spectral modification observed on J774 spectra in LDL medium. A shift and a larger band width were observed at this interval (Figure 7, II).

Surprisingly, the eigenvector of A3 (7.3%, Figure 7, III) reflects the contribution of the bands at 960-1000 cm^{-1} and 1050-1088 cm^{-1} attributed respectively to $\nu(\text{PO}_3^{2-})$ and to $\nu(\text{C-O})$ in DNA, RNA ribose [31]. Recording spectra on cytoplasm and nucleus was not possible in IR for J774 because the size of the macrophages was almost the size of one pixel. Murine macrophages are between 10 and 30 μm and tighten during cell culture cycles. A3 loading revealed a negative correlation of the band at 1720-1752 cm^{-1} , which showed a greater expression in EPA medium and in LDL medium. The score plot confirms this observation. This band was less intense in EPA/LDL medium. Score plots on A1, A3 and A2, A3 (data not shown) do not distinguish between standard and overloaded media. A3 component probably contains information related to the cell compartment (nucleus and cytoplasm) and A2 component separates LDL spectra from other media.

Score plot on A1 and A4 separates standard and overloaded media (Figure S4, c and d in supplementary data). A4 loading (4.2%, Figure 7, IV) shows a positive correlation of the bands at 1134-1206 cm^{-1} attributed to the $\nu_{\text{asym}}(\text{CO})$ of PLs ester and CE [31, 32], at 2838-2870 cm^{-1} and at 2894-2947 cm^{-1} which correspond respectively to the $\nu_{\text{sym}}(\text{CH}_2)$ and $\nu_{\text{asym}}(\text{CH}_2)$ in lipid and FA chain [31, 33]. These bands reflect lipid modifications and are overexpressed in overloaded media according to the score plot in the space of A1 and A4. Components A1, A2, A3 and A4 express 93% of the information from the IR dataset.

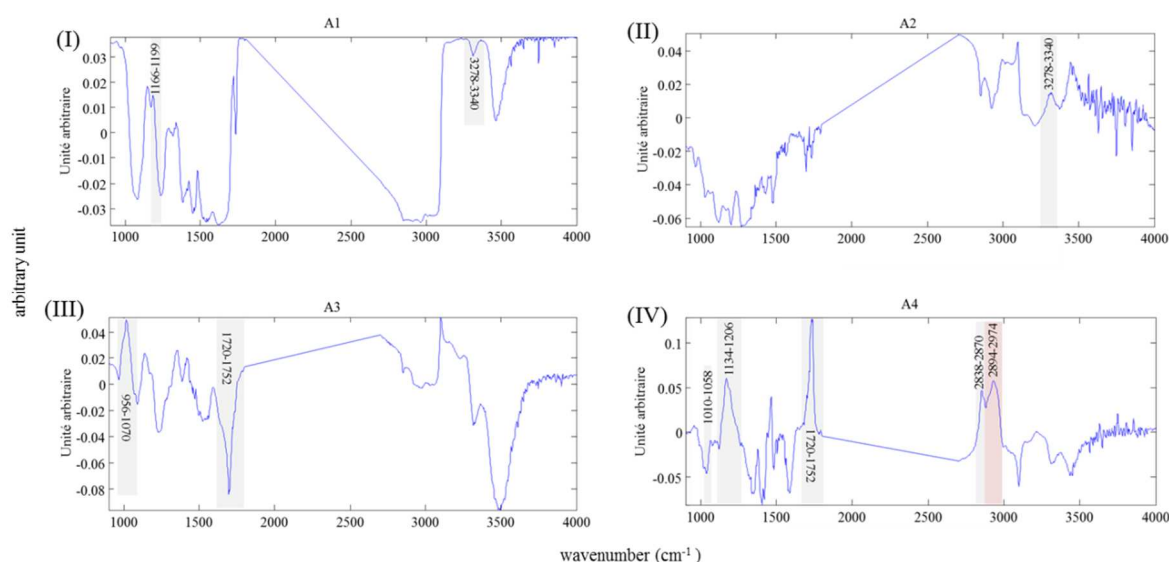


Figure 7 : Loadings of A1, A2, A3 and A4 principal components for IR data.

Discussion and conclusion

Atherosclerosis studies make a list of various *in vivo* imaging modalities used to better understand of the morphological changes accompanying the formation of atheromatous plaques, but do not give information about the chemical composition of these plaques. [1] Raman and infrared vibrational spectroscopies are suggested techniques for biochemical characterization of plaques *in vitro*. [13] Literature reports numerous studies on the contribution of Raman spectroscopy in the monitoring of lipids for various cell types involved in cardiovascular diseases: neutrophils, endothelial cells and macrophages [36]. In order to distinguish characteristic molecules from other lipids present and which respond spectroscopically, deuterium markings are often used [16, 37, 38].

In this work, the contribution of Raman and infrared vibrational techniques was evaluated on J774, overloaded, or not, with cholesterol by acLDL, in presence or absence of EPA.

Incorporation of EPA in J774 murine macrophages, in standard or overloaded media, reduces the activity of the extracellular transporter ABCA1; which implies the reduction of cholesterol efflux. The decrease in cholesterol efflux in macrophages leads to changes in neutral lipids (cholesteryl esters and triglycerides) and induces the formation of lipid droplets [6, 18]. Previous study based on a lipidomic approach and a series of biological tests investigated the molecular species involved in the modification of lipid composition and made it possible to identify changes in certain lipid classes, including phosphatidylinositol, phosphatidylethanolamine, phosphatidylcholine, and slightly less in sphingomyelin and phosphatidylserine. It is important to mention that phospholipids are abundant in macrophages [18].

In the present paper, vibrational spectroscopy revealed spectral changes following the enrichment of cells with fatty acids. In particular, we highlighted spectral changes in the spectral regions attributed to lipids (triglycerides, phospholipids and cholesterol) in both Raman and IR between standard and overloaded media. The contribution of the identified bands required additional statistical analysis.

Raman analysis makes it possible to differentiate between J774 cytoplasm and nucleus. Principal component analysis revealed the possibility through the third component to separate groups between standard and overloaded media. PCA asserted that dissimilarities between the four growth conditions are minimal. Nevertheless, it is possible to differentiate the four growth media based on the sixth component A6. Concerning the second order derivatives, characteristics vibrational bands related to the LDL medium are particularly highlighted.

In Raman imaging, the projection of the ratio of the bands at $2700\text{-}2800\text{ cm}^{-1}$ and $1645\text{-}1655\text{ cm}^{-1}$ corresponding respectively to the $\nu_{\text{sym}}(\text{CH}_2)$ in lipid and to Amide I shows a higher amount of lipids in the cytoplasm in overloaded media. In addition, CLS fitting on Raman images confirmed a more abundant distribution of lipids in the cytoplasm, especially for overloaded media. The lipid ratio is the highest in EPA/LDL medium. In the latter, J774 cells presented a higher ratio all over the cell even in the nucleus.

Principal component analysis on the IR spectra revealed that the first component provides information related to the presence of eicosapentaenoic acid EPA in the medium. The second component makes it possible to distinguish the spectra of the LDL medium from other media. The distinction between standard and overloaded media is possible through the fourth component.

Infrared spectroscopy confirmed the spectral changes observed in Raman following the enrichment of culture medium with FA. The vibrational band at 1732 cm^{-1} that corresponds to the $\nu(\text{C}=\text{O})$ in CE, FA and polysaccharides [21, 33] appears on the EPA, LDL, and EPA / LDL spectra. IR analysis provided additional information in the lipid region. Indeed, the band at $3280\text{-}3300\text{ cm}^{-1}$ is wider on the spectra of the LDL medium with a shift of about 10 cm^{-1} of the maximum. This shift is also observed in EPA/LDL medium where the maximum is at 3284 cm^{-1} . Still, the intensity of the band at $3280\text{-}3300\text{ cm}^{-1}$ for EPA/LDL is significantly lower compared to other growth media.

The analysis of macrophages by IR does not allow recording spectra on cell compartment. During the chemometric analysis, component A3 displayed information related to the nucleus and cytoplasm. Peritoneal macrophages have a diameter between 10 and 30 μm with nucleus dimensions between 6 and 12 μm [15]. In addition, the duration of culture cycles changes the shape of the macrophages and their diameter will be reduced to 15-18 μm [39]. By consequence, an infrared spectrum herein represents an entire macrophage. However, even if the spatial resolution is better in Raman, acquisition time of an image remains much faster in IR. The main advantage remains that both IR and Raman are non-destructive methods.

In conclusion, both Raman and IR techniques have advantages and disadvantages, give complementary vibrational data, and are complementary to other analytical tools. Herein, no cell labelling is used and the originality of the study is somehow to point spectral changes relying only on chemometrics.

In perspective, it is conceivable to test other macrophage lines and to optimize the preparation of the sample. Another alternative will be to perform Raman analysis on the cells directly in the culture medium using an immersion objective. This alternative is not possible in IR. In

addition, immersion analysis enables *in situ* monitoring of lipid droplets. The latter were observed in cells during this study. The contribution of vibrational techniques for the monitoring of intracellular lipid droplets and cells *in situ* seems promising.

Conflicts of interest

There are no conflicts to declare.

References

- [1] T.J. Romer, J.F. Brennan, 3rd, T.C. Schut, R. Wolthuis, R.C. van den Hoogen, J.J. Emeis, A. van der Laarse, A.V. Brusckhe, G.J. Puppels, Raman spectroscopy for quantifying cholesterol in intact coronary artery wall, *Atherosclerosis* 141(1) (1998) 117-24.
- [2] R.P. Choudhury, E.A. Fisher, Molecular imaging in atherosclerosis, thrombosis, and vascular inflammation, *Arterioscler Thromb Vasc Biol* 29(7) (2009) 983-91.
- [3] P. Libby, P.M. Ridker, G.K. Hansson, Progress and challenges in translating the biology of atherosclerosis, *Nature* 473(7347) (2011) 317-25.
- [4] K.J. Moore, F.J. Sheedy, E.A. Fisher, Macrophages in atherosclerosis: a dynamic balance, *Nat Rev Immunol* 13(10) (2013) 709-21.
- [5] A. Edsfeldt, P. Duner, M. Stahlman, I.G. Mollet, G. Ascitto, H. Grufman, M. Nitulescu, A.F. Persson, R.M. Fisher, O. Melander, M. Orho-Melander, J. Boren, J. Nilsson, I. Goncalves, Sphingolipids Contribute to Human Atherosclerotic Plaque Inflammation, *Arterioscler Thromb Vasc Biol* 36(6) (2016) 1132-40.
- [6] N. Fournier, S. Tardivel, J.-F. Benoist, B. Védie, D. Rousseau-Ralliard, M. Nowak, F. Allaoui, J.-L. Paul, Eicosapentaenoic acid membrane incorporation impairs ABCA1-dependent cholesterol efflux via a protein kinase A signaling pathway in primary human macrophages, *Biochimica et Biophysica Acta (BBA) - Molecular and Cell Biology of Lipids* 1861(4) (2016) 331-341.
- [7] G. Sayet, N. Fournier, E. Caudron, S. Tfaili, A. Solgadi, J.-L. Paul, P. Chaminade, Lipidomic study of the impact of eicosapentaenoic acid (EPA) on abca1-mediated cholesterol efflux from human macrophages, *Atherosclerosis* 263 (2017) e222-e223.
- [8] N. Fournier, G. Sayet, B. Védie, M. Nowak, F. Allaoui, A. Solgadi, E. Caudron, P. Chaminade, J.F. Benoist, J.L. Paul, Eicosapentaenoic acid membrane incorporation impairs cholesterol efflux from cholesterol-loaded human macrophages by reducing the cholesteryl ester mobilization from lipid droplets, *Biochim Biophys Acta* 1862(10 Pt A) (2017) 1079-1091.
- [9] K. Majzner, S. Chlopicki, M. Baranska, Lipid droplets formation in human endothelial cells in response to polyunsaturated fatty acids and 1-methyl-nicotinamide (MNA); confocal Raman imaging and fluorescence microscopy studies, *J Biophotonics* 9(4) (2016) 396-405.
- [10] K. Majzner, S. Tott, L. Roussille, V. Deckert, S. Chlopicki, M. Baranska, Uptake of fatty acids by a single endothelial cell investigated by Raman spectroscopy supported by AFM, *Analyst* 143(4) (2018) 970-980.
- [11] K. Kochan, E. Kus, E. Szafraniec, A. Wislocka, S. Chlopicki, M. Baranska, Changes induced by non-alcoholic fatty liver disease in liver sinusoidal endothelial cells and hepatocytes: spectroscopic imaging of single live cells at the subcellular level, *Analyst* 142(20) (2017) 3948-3958.
- [12] P.P. Toth, Subclinical atherosclerosis: what it is, what it means and what we can do about it, *Int J Clin Pract* 62(8) (2008) 1246-54.
- [13] J. Park, P. Pande, S. Shrestha, F. Clubb, B.E. Applegate, J.A. Jo, Biochemical characterization of atherosclerotic plaques by endogenous multispectral fluorescence lifetime imaging microscopy, *Atherosclerosis* 220(2) (2011) 394-401.
- [14] P.R. Moreno, R.A. Lodder, K.R. Purushothaman, W.E. Charash, W.N. O'Connor, J.E. Muller, Detection of lipid pool, thin fibrous cap, and inflammatory cells in human aortic atherosclerotic plaques by near-infrared spectroscopy, *Circulation* 105(8) (2002) 923-7.
- [15] J. Lam, M. Herant, M. Dembo, V. Heinrich, Baseline mechanical characterization of J774 macrophages, *Biophys J* 96(1) (2009) 248-54.

- [16] C. Matthäus, C. Krafft, B. Dietzek, B.R. Brehm, S. Lorkowski, J. Popp, Noninvasive Imaging of Intracellular Lipid Metabolism in Macrophages by Raman Microscopy in Combination with Stable Isotopic Labeling, *Analytical Chemistry* 84(20) (2012) 8549-8556.
- [17] L.J. Den Hartigh, J.E. Connolly-Rohrbach, S. Fore, T.R. Huser, J.C. Rutledge, Fatty Acids from Very Low-Density Lipoprotein Lipolysis Products Induce Lipid Droplet Accumulation in Human Monocytes, *The Journal of Immunology* 184(7) (2010) 3927.
- [18] N. Fournier, N. Attia, D. Rousseau-Ralliard, B.t. Védie, F.d.r. Destailats, A. Grynberg, J.-L. Paul, Deleterious impact of elaidic fatty acid on ABCA1-mediated cholesterol efflux from mouse and human macrophages, *Biochimica et Biophysica Acta (BBA) - Molecular and Cell Biology of Lipids* 1821(2) (2012) 303-312.
- [19] S.K. Basu, J.L. Goldstein, G.W. Anderson, M.S. Brown, Degradation of cationized low density lipoprotein and regulation of cholesterol metabolism in homozygous familial hypercholesterolemia fibroblasts, *Proceedings of the National Academy of Sciences of the United States of America* 73(9) (1976) 3178-82.
- [20] S. Tfaili, Caractérisation par microspectroscopie confocale Raman de la diffusion cutanée d'actif: optimisation des paramètres instrumentaux et méthodologiques en vue d'applications in vivo., Université de Reims Champagne-Ardenne, Reims, 2012.
- [21] A. Tfayli, Caractérisation structurale et moléculaire de la peau par microscopies optiques vibrationnelles, application diagnostic précoce des tumeurs cutanées et à l'étude de la diffusion de principes actifs à visée thérapeutique., Université de Reims Champagne-Ardenne, Reims, 2007.
- [22] F. Draux, P. Jeannesson, A. Beljebbar, A. Tfayli, N. Fourre, M. Manfait, J. Sule-Suso, G.D. Sockalingum, Raman spectral imaging of single living cancer cells: a preliminary study, *Analyst* 134(3) (2009) 542-8.
- [23] I. Notingher, S. Verrier, H. Romanskab, A.E. Bishop, J.M. Polakb, L.L. Hench, In situ characterisation of living cells by Raman spectroscopy, IOS Press (2002).
- [24] K. Czamara, K. Majzner, M.Z. Pacia, K. Kochan, A. Kaczor, M.C.J.-R. Baranska, Raman spectroscopy of lipids: a review, *Journal of Raman Spectroscopy* 46(1) (2014) 4-20.
- [25] C. Matthäus, C. Krafft, B. Dietzek, B.R. Brehm, S. Lorkowski, J. Popp, Noninvasive imaging of intracellular lipid metabolism in macrophages by Raman microscopy in combination with stable isotopic labeling, *Anal Chem* 84(20) (2012) 8549-56.
- [26] J. De Gelder, K. De Gussem, P. Vandenabeele, L. Moens, Reference database of Raman spectra of biological molecules, *Journal of Raman Spectroscopy* 38(9) (2007) 1133-1147.
- [27] D. Chaturvedi, S.A. Balaji, V.K. Bn, F. Ariese, S. Umapathy, A. Rangarajan, Different Phases of Breast Cancer Cells: Raman Study of Immortalized, Transformed, and Invasive Cells, *Biosensors (Basel)* 6(4) (2016).
- [28] A.F. Palonpon, J. Ando, H. Yamakoshi, K. Dodo, M. Sodeoka, S. Kawata, K. Fujita, Raman and SERS microscopy for molecular imaging of live cells, *Nat Protoc* 8(4) (2013) 677-92.
- [29] C. Matthäus, B. Bird, M. Miljkovic, T. Chernenko, M. Romeo, M. Diem, Chapter 10: Infrared and Raman microscopy in cell biology, *Methods Cell Biol* 89 (2008) 275-308.
- [30] A. Campion, Infrared and Raman Spectroscopy of Biological Materials. Practical Spectroscopy Series., *Journal of the American Chemical Society* 123(42) (2001) 10427-10427.
- [31] G. Bellisola, C. Sorio, Infrared spectroscopy and microscopy in cancer research and diagnosis, *Am J Cancer Res* 2(1) (2012) 1-21.
- [32] I. Dreissig, S. Machill, R. Salzer, C. Krafft, Quantification of brain lipids by FTIR spectroscopy and partial least squares regression, *Spectrochim Acta A Mol Biomol Spectrosc* 71(5) (2009) 2069-75.
- [33] A. Oleszko, S. Olsztynska-Janus, T. Walski, K. Grzeszczuk-Kuc, J. Bujok, K. Galecka, A. Czernski, W. Witkiewicz, M. Komorowska, Application of FTIR-ATR Spectroscopy to Determine the Extent of Lipid Peroxidation in Plasma during Haemodialysis, *Biomed Res Int* 2015 (2015) 245607.
- [34] A.M. Martelli, F. Fala, I. Faenza, A.M. Billi, A. Cappellini, L. Manzoli, L. Cocco, Metabolism and signaling activities of nuclear lipids, *Cellular and molecular life sciences : CMLS* 61(10) (2004) 1143-56.
- [35] K. Czamara, J. Natorska, P. Kapusta, M. Baranska, A. Kaczor, Raman microspectroscopy of human aortic valves: investigation of the local and global biochemical changes associated with calcification in aortic stenosis, *Analyst* 140(7) (2012) 2164-70.
- [36] B. Kann, H.L. Offerhaus, M. Windbergs, C. Otto, Raman microscopy for cellular investigations--From single cell imaging to drug carrier uptake visualization, *Advanced drug delivery reviews* 89 (2015) 71-90.

[37] C. Stiebing, C. Matthäus, C. Krafft, A.-A. Keller, K. Weber, S. Lorkowski, J. Popp, Complexity of fatty acid distribution inside human macrophages on single cell level using Raman micro-spectroscopy, *Analytical and Bioanalytical Chemistry* 406(27) (2014) 7037-7046.

[38] C. Stiebing, L. Schmolz, M. Wallert, C. Matthaues, S. Lorkowski, J. Popp, Raman imaging of macrophages incubated with triglyceride-enriched oxLDL visualizes translocation of lipids between endocytic vesicles and lipid droplets, *J Lipid Res* 58(5) (2017) 876-883.

[39] M.A. Elhelu, The role of macrophages in immunology, *J Natl Med Assoc* 75(3) (1983) 314-7.